Comparing the standard and de Sitter interpolations for MOND by testing on globular clusters with an N-body code

J.H.C. Gommers

BSc Thesis: Applied Physics, TU Delft
Supervisors: S.W.H. Eijt, P.M. Visser

2nd July 2025

Abstract

MOdified Newtonian Dynamics (MOND) is an alternative explanation for the rotation-distance curves of galaxies that modifies Newton's law for gravity at low gravitational accelerations, opposing dark matter. Since its initial proposal, many interpolation functions for MOND have been proposed.

One potential interpolation function is the de Sitter interpolation, based on the properties of the de Sitter space. It is newly tested on globular clusters through simulation in this thesis. A simulation is needed because no analytical solution exits. Although the de Sitter interpolation function is quite old, limited research has gone into it so far.

In this thesis, the credibility of this function will be examined by comparing it to one of the most popular functions: the standard interpolation. It will be tested on two globular clusters (NGC 6101 and NGC 5466), using the approximation of an isothermal sphere for initialization and an N-body particle mesh code to simulate the systems according to the gravitational law obtained through both of these functions. Afterwards, the resulting star density and velocity dispersion, both as function of distance to the centre of the cluster, will be compared to their observed counterparts.

The credibility of the results will be discussed in depth, comparing the system to the isothermal sphere, considering what changes variations in the parameters cause and assuring the system is in equilibrium after simulation.

The results show the de Sitter interpolation is on par with the standard interpolation, producing very similar results. Both match very well to the observed star count densities, and the velocity dispersion of NGC 6101 matches well to the observations too, whereas the velocity dispersion of NGC 5466 does not, in which case both functions match equally badly and predict a too high velocity dispersion.

In short, this thesis proves the usability of the de Sitter interpolation on globular clusters approximated as isothermal spheres, but further research is required to prove or disprove its superiority - in terms of its ability to match the observations - to the standard function.

1 Introduction

For a long time now, it has been well established that the visible (baryonic) matter in the universe does not behave in accordance with Newton's law for gravity, when one assumes all mass in the universe is baryonic. Phenomena such as flat rotation curves, too high relative speeds between galaxies, too strong gravitational lensing and much more, all points to the existence of unobserved mass (McGaugh, 2021a). When dark matter was first proposed, it could have consisted of many hard to detect baryonic sources of mass; neutrinos, gas, faint stars, black holes or planets. But through observations it has been determined that none of these sources, nor their sum, could make up the discrepancy. This leads, by necessity when Newton's laws are assumed as true, to some unknown non- or weakly interacting particle, which is how dark matter is understood (McGaugh, 2021a).

However, there are also issues that this dark matter cannot explain. The Tully-Fisher relation is one such example (McGaugh, 2021b), the stability of galaxies another, or the rotation in barred galaxies (Roshan et al., 2021). Much research has also gone into attempts to find dark matter, but all attempts so far have been unsuccessful (Astroweb, retrieved 2025).

That is why Milgrom invented and published his alternative idea: MOND, MOdified Newtonian Dynamics. It proposes alternate gravitational behaviour

(or an alternate understanding of inertia, but this will not be considered in the scope of this thesis) in the low acceleration limit only. There is no reason after all, to believe that Newton's law is not an excellent approximation in the high-acceleration-regime.

MOND is able to explain most of the discrepancies that dark matter explains: The shape of the velocity dispersion, the stability of galaxies, the strength of the gravitational lensing, the temperature of intracluster gas and the relative speeds of galaxies can all be explained by MOND as well (McGaugh, 2021a). An exception to this is the bullet cluster, where more mass than observed is needed to make things work, either in MOND or in Newton. However, this could be unobserved baryonic mass (Milgrom, 2015). Meaning, all this is without the need for any additional non-interacting mass (Milgrom, 2001).

To reconcile the two regimes, an interpolation - which is able to describe gravity at *every* acceleration - is needed. Many interpolations have previously been suggested, but in this thesis, two will be tested: the standard interpolation function and a less well-known one, based on the de Sitter space, both proposed by Milgrom (Milgrom, 1999).

These tests will be executed using a previously developed N-body particle mesh code by (de Nijs et al., 2024). The model will be applied on the observed physical parameters of a selection of globular clusters, and the result will be a velocity dispersion and a mass distribution of each cluster, both as function of distance to the centre, and both of which can be compared to their observed counterparts.

Globular clusters are small galaxies, in the order of 10^5 stars, that are distributed approximately spherically symmetrically. The ones examined in this thesis all orbit the Milky Way, meaning they are quite nearby on a cosmological scale and observations are fairly precise. Globular clusters will be tested because they often have both a Mondian and Newtonian component (meaning parts of the galaxy where either approximation works well), meaning that there must also be a region where the interpolation is necessary. Apart from that, globular clusters behave similarly to isothermal spheres, for which an analytical solution exists in the deep MOND regime. This solution can be used both as a sanity check, and an initial state. These similarities are in the randomness of direction of motion, the shape and the mass distribution.

Ideally, the clusters will be chosen to represent both approximations, deep MOND and Newton, as well as the transition regime, by selecting ones with parameters that give dominant components in one of them.

The fact that these clusters all orbit the Milky Way means they experience a significant external field effect from the gravity of the central galaxy. In this thesis, it will be considered if this effect is significant enough that it should be taken into account.

2 Physical background

2.1 MOND

MOND introduces a new constant with the dimensions of an acceleration, a_0, such that the standard Newtonian law of gravity is a good approximation only for accelerations $a \gg a_0$. In the opposite limit, $a \ll a_0$, the following applies to a spherically symmetric system (Milgrom, 2001):

$$\frac{a^2}{a_0} = \frac{MG}{r^2} \tag{1}$$

In eq (1), a is the deep MOND gravitational acceleration, M is the mass enclosed by a sphere with radius r, G is the gravitational constant and r is the distance to the centre of the cluster.

Several values of the parameter a_0 have been proposed, always in the order of magnitude of 10^{-10} m/s^2, and have been established in many different ways. These ways include observation of rotation curves of different galaxies and star clusters, the velocity of galaxies in galactic clusters, from the Hubble constant and from the cosmological constant (Milgrom, 1983b). The best estimation today, based on fits, is $1.2 \cdot 10^{-10}$ m/s^2 (McGaugh et al., 2016) and (Lelli et al., 2017). This is the value that shall be used for a_0 in this thesis.

The Newtonian and Mondian expressions can be interpolated around $a = a_0$ as (Milgrom, 2001):

$$\mu\left(\frac{a}{a_0}\right) a = \frac{MG}{r^2} \tag{2}$$

In eq (2) and everywhere else from here on, a is the gravitational acceleration at any point in the combined regime. $\mu(x)$ is an interpolation function that satisfies $\mu(\mathrm{x}) \to 1$ for $x \gg 1$ and $\mu(x) \to x$ for $x \ll 1$. (Milgrom, 2001)

The following partial differential equation describes the Mondian potential:

$$\nabla \cdot (\nabla\phi\mu\left(\frac{|\nabla\phi|}{a_0}\right)) = 4\pi G\rho_B(\mathbf{r}, t) \tag{3}$$

This is used in the algorithm of the N-body code.

The interpolation function can take any smooth shape that satisfies the two limits, there is no theory

stating it should be one in particular. One of the most popular functions is the standard interpolation function. Many previous examinations have found this function to match well to the observational data.

$$\mu(x) = \frac{x}{\sqrt{1+x^2}} \tag{4}$$

$$\nu(y) = \sqrt{\frac{1}{2} + \frac{1}{2}\sqrt{1+\frac{4}{y^2}}} \tag{5}$$

Eq. (4) is the standard interpolation function, and eq. (5) the inverse of it, the inverse is defined so that $\mu(x)x = y$ and $\nu(y)y = x = \frac{a}{a_0}$. It is needed to retrieve the Mondian acceleration from x.

One of many alternatives is the de Sitter interpolation, named for the de Sitter space it is based on.

$$\mu(x) = \frac{\sqrt{1+4x^2}-1}{2x} \tag{6}$$

$$\nu(y) = \sqrt{1+\frac{1}{y}} \tag{7}$$

Milgrom has pointed out that the de Sitter space might be able to explain Mondian behaviour (Milgrom, 1999). The paper posits a_0 is very close in value to cH_0, where c is the speed of light and H_0 the Hubble constant, as well as to $c^2(\Lambda/3)^{1/2}$. Here, Λ is the cosmological constant. This means there might well be a physical connection between MOND and a_0 on one hand and the cosmological constant and/or the expansion of the universe on the other (Milgrom, 2009).

In five-dimensional Minkowski space-time - of which the de Sitter space is a submanifold, there exists the five-acceleration (Smolin, 2016) and (Milgrom, 1999):

$$a_5 = \sqrt{\left(c^2\sqrt{\frac{\Lambda}{3}}\right)^2 + a^2} \tag{8}$$

This can be equalled to $\mu(x)x$ to derive the interpolation function. This function is not unique, but can be chosen so that the requirements posed by MOND are met. Eqs (6) and (7) are the result.

In this thesis, these two interpolations will be compared, as well as the deep MOND situation, meaning that $\mu(x) = x$.

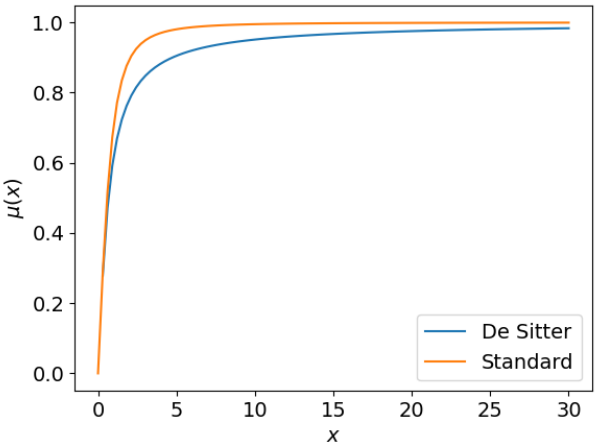

Figure 1: *Comparison of the two selected interpolation functions in the domain (0,30).*

As can be observed in Fig 1, the de Sitter interpolation transitions a lot slower than the standard function. This might mean the results will be visibly different between the two.

2.2 Initial distribution: isothermal sphere

It has previously been proven that models based on an isothermal sphere, such as the King model - which is a model based on the isothermal sphere approximation, derived from Newton's laws - are very good approximations of globular clusters (Madson, 1996), though to make sure the simulation behaves as expected, the results can be compared against these analytical ones.

In perfect thermodynamic equilibrium, with an infinite number of particles with equal masses, in the deep MOND regime, it holds that: (de Nijs et al., 2024)

$$M(r) = \frac{Mr^3}{b^3}\left(1+\frac{r^{3/2}}{b^{3/2}}\right)^{-2} \tag{9}$$

$$\frac{3k_BT}{2m} = \frac{\langle v^2\rangle}{2} = \frac{\sqrt{GMa_0}}{3} \tag{10}$$

In eq (9), b is a measure for the size of the cluster, it is the quarter-mass radius, the radius a sphere of which encompasses a quarter of the total mass. It is proportional to the half-mass radius by a factor, which in this model is 0.556. In eq (10), k_B is the Boltzmann-constant, T is a measure for the random movement of the particles, not the actual temperature, m is the mass of one particle, $\langle v^2\rangle$ is the average squared speed, M is the total mass of the cluster. Eq. (10) can be used to rewrite the Maxwell-Boltzmann velocity distribution so that it

depends only on a root-mean square velocity and the velocity of a particle.

$$p(\mathbf{v}) = \left(\frac{2\pi\langle v^2\rangle}{3}\right)^{-\frac{3}{2}} e^{-\frac{3\mathbf{v}\cdot\mathbf{v}}{2\langle v^2\rangle}} \tag{11}$$

$p(\mathbf{v})$ is the probability density that a particle has velocity $\mathbf{v}$. The average speed satisfies $v_{RMS} = \sqrt{\langle v^2\rangle}$, which can be calculated using eq (10) using the mass of the system.

These distributions, combined with the parameters of the cluster, will be used to initialize the system so that it starts close to the equilibrium state and little time is needed to move toward it.

In this isothermal sphere for deep MOND, the 3D mass density can be established analytically too (de Nijs et al., 2024).

$$\rho_B(r) = \frac{3M}{4\pi b^3}\left(1 + \frac{r^{3/2}}{b^{3/2}}\right)^{-3} \tag{12}$$

This means in the tail, where the acceleration is very low and deep MOND is expected to be a good approximation, the density should fall off with $r^{-9/2}$.

2.3 How clusters will be selected

The interpolation function should encompass all regimes, as it converges to the Newtonian regime and the Mondian regime for $a \gg a_0$ and $a \ll a_0$ respectively. To examine the applicability of the functions, it is therefore important to test it in all three regimes, also including the regime close to the transition.

Clusters are often largely in one regime or the other, with only small parts in the transition. How Mondian or Newtonian it is (or what the values of x are throughout the system) can be calculated from the accelerations. But that requires simulations first. To be able to select the clusters upfront, the approximation of the isothermal sphere in deep MOND will again be used.

$$\left|\frac{a}{a_0}\right| = \sqrt{\frac{GM}{a_0}} b^{-\frac{3}{2}} \frac{r^{\frac{1}{2}}}{1 + (\frac{r}{b})^{\frac{3}{2}}} \tag{13}$$

From eq (13), the maximal acceleration can be calculated by differentiating over r and equalling the result to 0. At this maximal acceleration, $a_{\max}$, the following holds:

$$\left|\frac{a_{\max}}{a_0}\right| = \frac{2^{\frac{2}{3}}}{3}\frac{\sqrt{\frac{GM}{a_0}}}{b} \equiv A \tag{14}$$

The dimensionless maximum acceleration will be called A from now on. If $A < 1$, then $a < a_0$ at all points of the cluster, meaning it is dominantly Mondian. For a value of $A \approx 1$, there will also be a considerable component in the transition regime. If $A \gg 1$, it will have a dominant Newtonian component, although also a Mondian one and one in the transition regime.

2.4 Description of the Simulation

Here will be described a short version of how the N-body mesh code functions. A more detailed version can be read in (de Nijs et al., 2024). The code can be accessed on `https://github.com/Joost987/MONDPMesh`.

The code first creates an initial state where each particle is assigned a randomly distributed velocity and position. This initial state is based on the isothermal sphere for deep MOND, as described in sec 2.2, one parameter for the position: the quarter-mass radius of the system, and one parameter for the velocity: the total mass.

The program treats each particle as having equal mass. The mass of each of the particle is spread out over a sphere, following a Gaussian distribution with a standard deviation of 1 pixel. This spreading is performed to counteract the effect of close encounters: Very high accelerations can be generated when two particles are close to each other. At the next step, the particle should be accelerated in the direction of the centre of the system, but if the next step is too temporally distant, the particle will already have moved outside the system, or have moved to a high-velocity orbit. By spreading the particles out over multiple pixels, when two would get very close to each other, they exert reduced net force on the other. Nevertheless, this was found to be a constraining factor in performing the simulations.

Then, all the simulations are performed, one timestep at a time. An iterative calculation is performed as follows: the Newtonian acceleration in each pixel is calculated from its deterministic function, and from it is calculated a vector field that consists of the Newtonian field and an orthogonal component. From this field and the inverse interpolation function, the Mondian vector field can be calculated. This field is projected onto a curl-free part, and now it can be used to calculate the Newtonian vector field with orthogonal component. From this, the orthogonal component alone is found which can be projected onto the divergence-free part, and this is then used to construct the new vector field of the combined Newtonian and its orthogonal acceleration. All these calculations are performed in the Fourier-domain for

fast computing. This whole process is repeated a preset number of times, that needs to be sufficient for the result to be close enough to both the analytical solution (for a system where one exists) and to stability, meaning the system doesn't change with increasing number of iterations.

The acceleration field is used to update the velocities and they to update the positions using the leapfrog method. These velocities and positions at the end of the simulation are treated as the state in which the system would be according to the law tested in that simulation.

The final results of the simulation are a set of matrices that include the whole system at each simulated time, showing 3D velocity and position of each particle, and the different energies and the angular momentum and linear momentum in the whole system at each time. It also returns all of that for the analytical solution, if it is available, meaning it is simulated in deep MOND with no external field effect (de Nijs et al., 2024).

The whole code has been optimized by (Koster, 2024) so that it performs the computations in parallel using the GPU, rather than the CPU which Python would use by default. Performance is still PC dependent, the specs of the PC used can be seen in sec 8.2

3 Finding Parameters

To be able to obtain good results from the simulations, a plethora of parameters is needed. The numbers of particles and pixels, the size of the pixels, the number of timesteps and their length, the number of iterations per timestep, the mass and quarter-mass radius of the cluster, the distance between the cluster and the sun and the centre of the Milky Way and the observed number of stars. These parameters include both the observed physical parameters of the globular clusters as well as ones that are related to the simulation and the spatial and temporal pixelation of the system. The former group will be found by considering experimental values of previously examined clusters to find a selection representative of all three regimes: deep MOND, Newtonian and the transition between the two.

An overview of all chosen parameters can be seen in sec 8.3.

3.1 Physical parameters

As described in section (2.3), the parameter A takes a value close to 1 when it has both a Newtonian and Mondian component, if $A \gg 1$, it is expected to be in the Newtonian regime and if $A \ll 1$ it can be considered to be in deep MOND everywhere. So the aim was to find one cluster with each of these values. Unfortunately, in practice it turned out hard to simulate clusters with high A, as the parameters of these systems caused them to easily explode and thus demonstrate non-physical behaviour. This behaviour can be seen in sec 8.1 The required number of timesteps to compensate made the simulations take longer than permissible. Therefore, only the domains $A \ll 1$ and $A \approx 1$ will be considered in this thesis.

It is also important that a mass distribution or mass density function, as well as a velocity profile have been created based on observational data.

The selected clusters are NGC 6101 with $A = 1.04$ (Baumgardt et al., retrieved 2025) and NGC 5466, which has $A = 0.569$ (Baumgardt et al., retrieved 2025).

To run the simulation, only the total mass of the system and the quarter-mass radius, which will be derived from the half-mass radius, are needed. Both of these values are provided by (Baumgardt et al., retrieved 2025), and are based on a best fitted King model. To inspect the need to include the external field effect from the Milky Way, the galactocentric distance (the distance between the cluster and the centre of the Milky Way) is also required. But for processing the results, the distance to the sun and observed number of stars are also needed. The number of stars is needed because it is convention to express a mass density in number of stars. This means this number is not the total number of stars in the system, but the total star count in the member selection of (de Boer et al., 2019), whose star density distribution will be used to compare against.

It is important to note that the simulations will be performed with very high mass per particle: 17 or 5.6 $M\odot$ per particle, as will be explained in sec 3.2, whereas the mass of stars in globular clusters is typically below 1 $M\odot$ (Baumgardt et al., 2023). This means that one particle is not 1 star, but a representation of a multitude of stars. The mass per star in the count is even higher, but this is of course because the number of stars in the selection is not nearly the total number, which would be in the order of 10^5.

It will also be considered if the external field effect could have a significant influence on the simulation, for which the stellar mass of the Milky Way is also needed, as this will be the largest contributor to the effect. $M_{MilkyWay} = 4.6 + 2.0/ - 1.3 \cdot 10^{10} M\odot$ (Licquia and Newman, 2013).

Cluster	Total mass [10^4 M⊙]	Half-mass radius [pc]	Galactocentric distance [kpc]	Distance to Sun [kpc]	Number of stars [-]
NGC 6101	17	13.87	10.360	14.450	1750
NGC 5466	5.6	13.75	16.480	16.120	1007

Table 1: *Used parameters of the clusters. All data from (Baumgardt et al., retrieved 2025), except the considered number of stars (not the total number) by (de Boer et al., 2019).*

3.2 Simulation parameters

The number of particles would, to ideally model the system, corroborate with the number of stars, but as this number is typically in the order of magnitude of 10^5 and the simulation time scales with N^2, where N is the simulated number of particles, this is unfeasible. Instead, N has been pinned to 10^4, which has previously been proven to already be a good approximation of the isothermal sphere for this mesh code (de Nijs et al., 2024). It has also been found to have an acceptable simulation time of two hours with all other parameters as described in this chapter.

The same research also proved four iteration steps were needed to get an error (deviation from the analytical solution of the isothermal sphere) $\leq$ 1 %. To prove this is a sufficient number, six iterations were also tested and compared against the four iterations, as can be seen in figure (2).

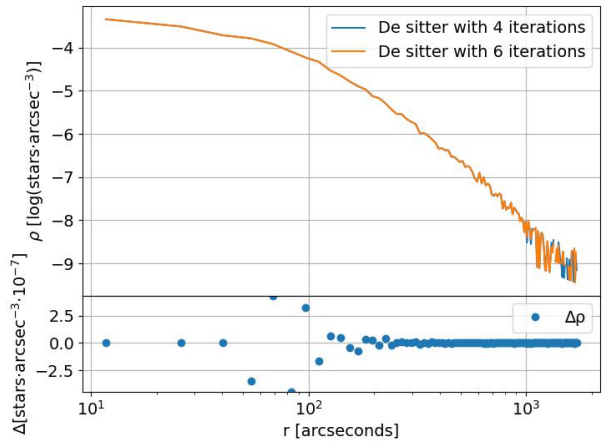

Figure 2: *3D star density of NGC 6101 simulated with the de Sitter interpolation with four and six iterations per timestep. It also shows the absolute difference between the two.*

To determine the needed timescale, a mass density plot of different simulated times was made, this means the other parameters were already needed: they have been chosen over an iterative process.

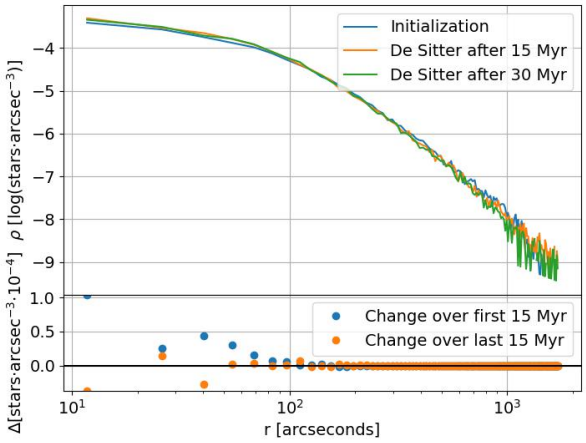

Figure 3: *3D-mass density of NGC 6101 at three times, and the changes between these snapshots. Simulation with the de Sitter interpolation.*

As can be seen in Fig 3, after 30 Myrs, $\Delta_{1,max} < 0.1 \cdot \Delta_{2,max}$, where subscripts 1 and 2 denote the first and second half of the simulated time. Similar plots have been made for the other tested regimes for both clusters, from which it was concluded that 30 Myr is a sufficient simulation time to reach a close-to equilibrium state, when using the isothermal sphere-distribution for deep MOND as start condition.

A constraint is put upon the number of timesteps by the necessity that the length of these steps is not too long. There is no hard definition for what too long is, but explosions caused by close encounters, as described in sec 2.4, are a clear indicator the timesteps of that simulation were chosen too large. This would be recognized as happening when all particles would suddenly leave the system, or the average velocity would suddenly change radically. The effect can be seen in figs 19 and 20. When this occurred, the timesteps were known to be chosen too long, and then more steps were needed so that each is smaller. Through a process of trial-and-error, a number of 6000 steps has been found to usually give stable results.

The number of pixels per half-axis has been found to be the most problematic. Ideally, it would be quite high to allow for a high resolution. This means the potential, and with that the acccelleration, can be accurately determined for each particle. However, to force physical behaviour, the particle distribution must be smooth, meaning that an increase in resolution demands an increase in number of particles. In this thesis, it has also been found experimentally, though with no explanation, that a greater number of pixels causes an explosion much

easier, to prevent this, a larger number of timesteps is also needed. And a greater number of pixels itself also requires more computing. All this means that the possible number of pixels is very much limited by the computational power of the used PC (specs described in sec 8.2). 64 pixels per half-axis of the simulated box is found to be the most achievable within a few hours of computing.

The ratio between quarter-mass radius and half-length of the box was similarly established: for a too large ratio, the particles could easily leave the system. But b should not be chosen too small in comparison to the box as this comes at the cost of spatial resolution. $b = \frac{1}{10} \cdot \frac{L}{2}$ was found to work well. It has been compared to $b = \frac{1}{20} \cdot \frac{L}{2}$, and an attempt has been made to compare it to $\frac{9}{50} \cdot \frac{L}{2}$. Here, $\frac{L}{2}$ is the half-length of the simulated box. However, it was found that in the last case, the cluster gets too close to the edge causing the system to easily explode, meaning an unfeasible number of timesteps was needed.

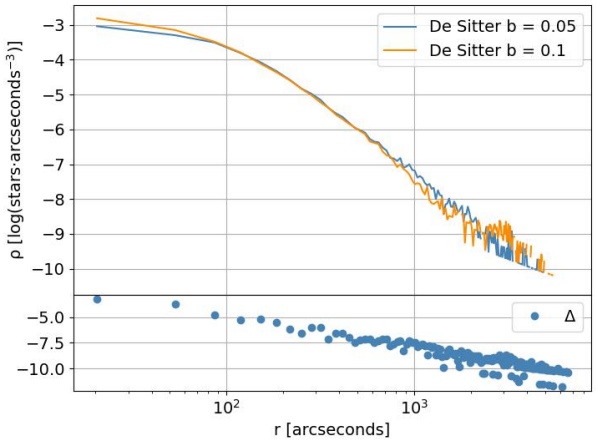

Figure 4: *3D star density of NGC 6101 with* $b_{frac} = 0.1$ *compared to* $b_{frac} = 0.05$ *after a de Sitter interpolation simulation. The difference has the same units as the densities.*

Since $b = \frac{1}{10} \cdot \frac{L}{2}$ is feasible and offers a higher resolution than the alternative considered, it will be used. Fig 4 demonstrates that, although there are considerable differences caused by the ratio between b and the size of the box, the result will largely follow the same pattern. It is as good as certain an even higher resolution will further improve results when paired with required increase in timesteps and number of particles, but the chosen ratio will have to do.

The isothermal distribution for deep MOND is used as an initial state because the analytical solution of the deep MOND regime is found to be a good approximation, supported by Fig 3. Although it is a solution of the deep MOND regime, it is also found experimentally to be a good start (meaning already close to the equilibrium state) for the transition regime, and will therefore be used as an initial state in testing the interpolation functions as well, by lack of an analytical solution.

4 Preliminary tests

In this chapter, the reliability of the simulations will be examined by comparing to analytical solutions, considering stability in time and considering the smoothness of the distribution. After that, the central density will be compared to the theoretical value. It will also be checked that the total energy remains constant. The need to examine the external field effect will also be considered here.

4.1 Analytical solutions

The deep-MOND simulations should resemble the deep MOND isothermal sphere closely, as that is the solution for an infinite number of particles.

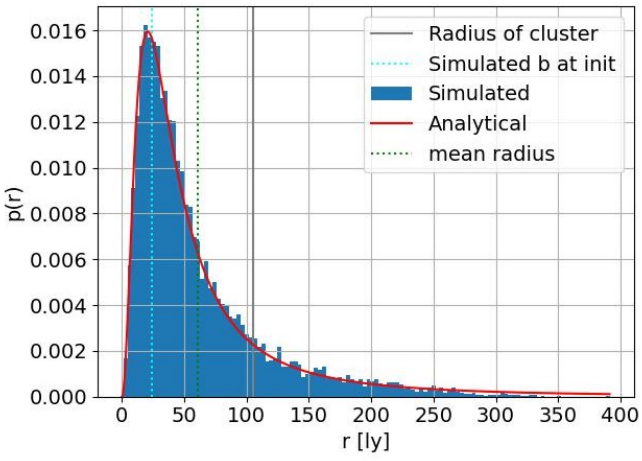

Figure 5: *Probability density against 3D radius of NGC 6101 at initialization. p(r) is the local mass in the bin with width dr, divided by the total mass and the binwidth, or* $\frac{1}{M}\frac{dM(r)}{dr}$

.

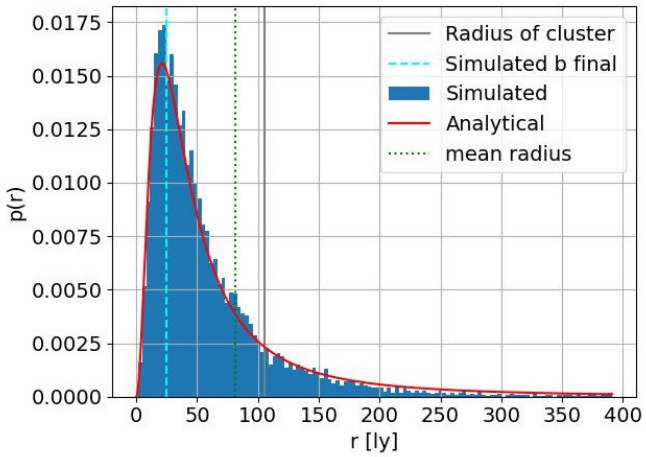

Figure 6: *Probability density against 3D radius of NGC 6101 after a simulation in the deep MOND regime. p(r) is the local mass in the bin with width dr, divided by the total mass and the binwidth, or* $\frac{1}{M}\frac{dM(r)}{dr}$.

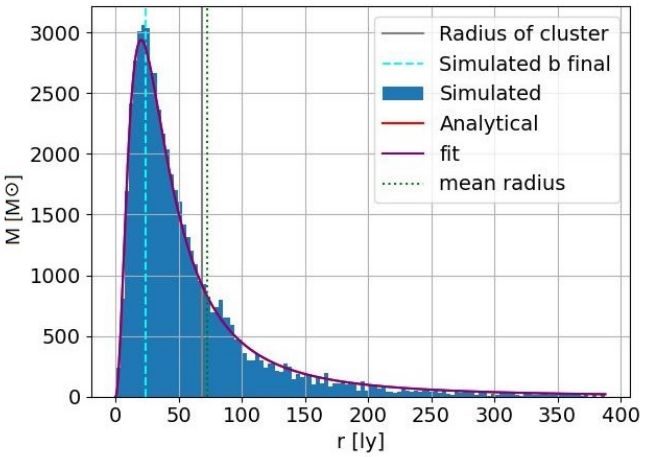

Figure 7: *Mass per bin, dM(r) against 3D radius of NGC 5466 after a simulation with the de Sitter interpolation, also including a curve fit.*

In Figs 5 and 6, analytical indicates the analytical solution of the isothermal sphere for deep MOND, the shape of which depends only on the quarter-mass radius. This can be found by taking the point at which a quarter of the points are included. The quarter-mass radius can also be found from a curve fit and the prompted value. These values were considered and it was found that this gives extremely close results to the number of points method, with no more than a 0.8% discrepancy between the two after-simulation methods, and often less. The largest difference between observed radius and simulated is 12.8 %.

Cluster	Interpolation	b (obs)	b (sim)	b (sim,iso)
NGC 6101	de Sitter	25.14	21.91	21.95
	Standard	25.14	22.88	22.85
	deep MOND	25.14	24.54	24.68
NGC 5466	de Sitter	24.92	23.49	23.46
	Standard	24.92	23.97	24.16
	deep MOND	24.92	24.70	24.73

Table 2: *Three quarter-mass radii per interpolation function, one as observed and prompted, one the point enclosing a quarter of the particles after simulation, and one by curvefitting the analytical solution for the deep MOND isothermal sphere to the simulated data.*

Figs 5 and 6 demonstrate that the initialization works, but also that the deep MOND simulation is not perfect, since after the simulation, the points are no longer distributed isothermally in the deep MOND regime. Nevertheless, the two are quite comparable. More iteration steps or a larger number of particles might be needed to better approximate an isothermal sphere, but because of constraints in simulation time, it will not be done.

The analytical solution can also be simulated in the deep MOND-regime, not using iterations, but direct calculation. The acceleration of the analytical solution should behave similarly to that of the iterative simulation, and this is demonstrated by Fig 8, the plot of the orbits calculated in these two ways of a single arbitrary particle, which are determined by the time-dependent acceleration.

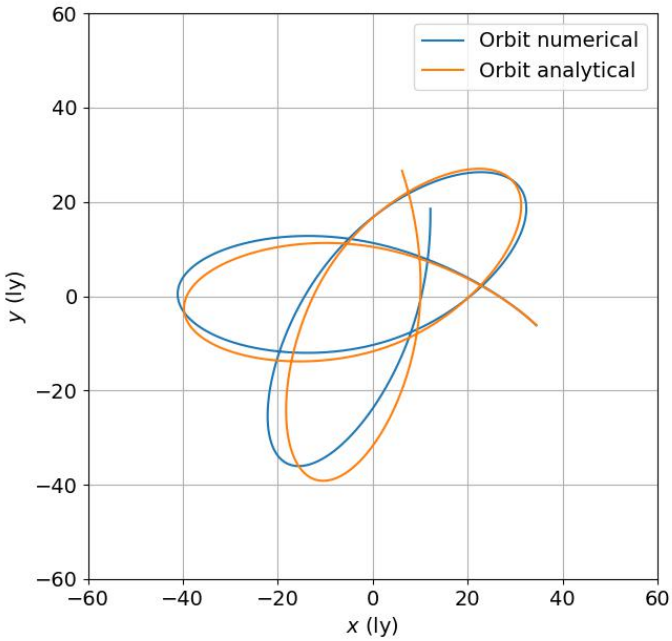

Figure 8: *Projection of the numerical and analytical orbits on the x,y plane of a specific particle in the deep MOND regime in NGC 5466.*

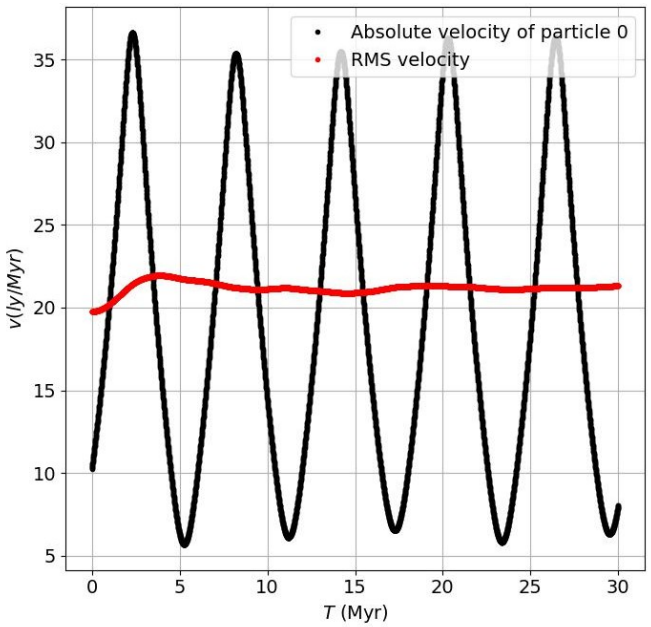

Figure 9: *Root mean square velocity, v_{RMS}, of the whole system over the simulated period (red), as well as the velocity of a single, arbitrarily chosen, particle. Simulated with the de Sitter interpolation for cluster NGC 6101.*

The slope of the density functions should be $-\frac{9}{2}$ on $\log_{10}$-scale, see sec 2.2. The slope in Fig 4 is estimated as -4.98 ± 0.9. Here, the uncertainty is caused by the noise in the tail. A slope of -4.5 falls within the margins.

Fig 9 demonstrates v_{RMS} quickly oscillates to a stable point and then proceeds to keep to that value with only slight variations. The single particle also oscillates with near-constant amplitude and frequency after a change early in the simulation.

4.2 Time stability

Fig 3 already shows the mass distribution undergoes most change in the first half of the simulation. The stability of the velocity dispersion will be futher demonstrated below.

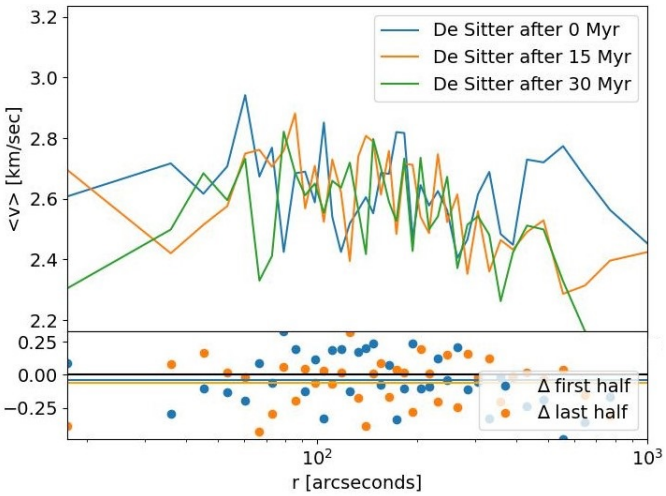

Figure 10: *1D velocity dispersion, $\sqrt{\langle v_x^2 \rangle}$, of NGC5466 simulated with the de Sitter interpolation.*

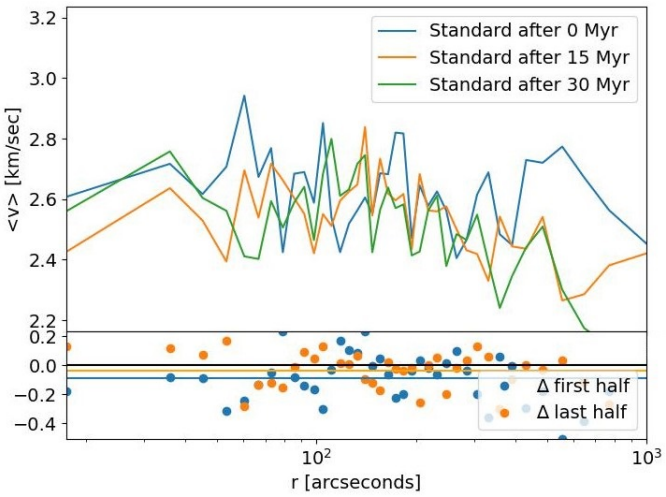

Figure 11: *1D velocity dispersion, $\sqrt{\langle v_x^2 \rangle}$ of NGC 5466 simulated with the standard interpolation.*

Figs 10 and 11 show the binned velocity dispersions against radius at different times, as well as the difference between the times. The horizontal lines are average changes, $\langle \Delta \rangle$, over the whole system. Surprisingly, the change is bigger in the second half for the de Sitter simulation in NGC 5466, Fig 10, though not for any other simulations. This does not indicate the total timescale is too small, as the expected change would still be less in the second half if that were the case.

As the changes, in all simulations, are quite small compared to the average velocity dispersion - in the order of a thirtieth - it is deemed no cause for concern, and the changing velocities will be ascribed to the continuous movement and interaction of particles, which happens also in equilibrium.

From all these plots, it can be safely concluded that the systems are indeed in equilibrium after a simulated time of 30 Myrs.

4.3 Smoothness of distribution

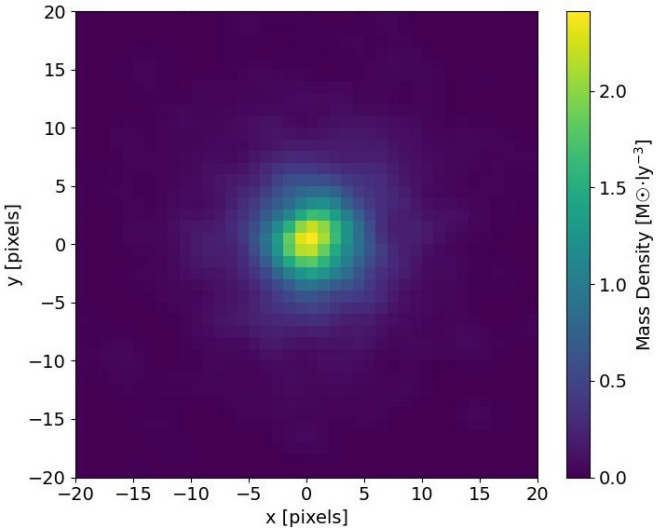

Figure 12: *Cross-sectional density at $z = 0$ per pixel of the NGC 6101 cluster after de Sitter interpolation simulation.*

Fig 12 shows the smoothness in distribution of the particles, which is needed to suppress the self-gravity caused by the discretization of the system (de Nijs et al., 2024). Clearly, there are no empty pixels in between filled ones, and the density decays gradually from the centre going outwards.

The central density is a bit lower than the deep MOND analytical solution of the isothermal sphere poses: 2.3 against 2.55 $M\odot \cdot \text{ly}^{-3}$. This discrepancy could as well be a difference with respect to the deep MOND isothermal sphere approximation, as an error through the simulation or the binning of masses in one pixel.

4.4 Central density

Here shall be expanded upon the concept of considering the density in the centre of the system.

$$\rho(0) = \frac{3M}{4\pi b^3} \tag{15}$$

Eq (15) (de Nijs et al., 2024) can be derived from the analytical solution of the density in deep MOND for an isothermal sphere by simply filling in $r = 0$. The densities obtained through simulation can be compared to these values to make sure they are trustable. This can be calculated in two ways: the density in the most central bin, the truest to the simulation, but influenced by the number of bins. Or alternatively, the analytical solution of the isothermal sphere can again be used with the radius containing

a quarter of the total points after simulation. The results of this can be seen in the table below.

Cluster	Method	ρ(0) points	ρ(0) isotherm
NGC 6101	Analytical		2.55
	De Sitter	3.73	3.86
	Standard	2.56	3.39
	Deep MOND	1.98	2.75
NGC 5466	Analytical		0.86
	De Sitter	0.90	1.03
	Standard	0.70	0.97
	Deep MOND	0.79	0.89

Table 3: *Analytical central densities from the isothermal sphere approximation for deep MOND, as well as the simulated values. Points is the density at the innermost bin. Isotherm is simulated using the isothermal sphere approximation. All values are in units of* $M\odot \cdot ly^{-3}$

4.5 Energy

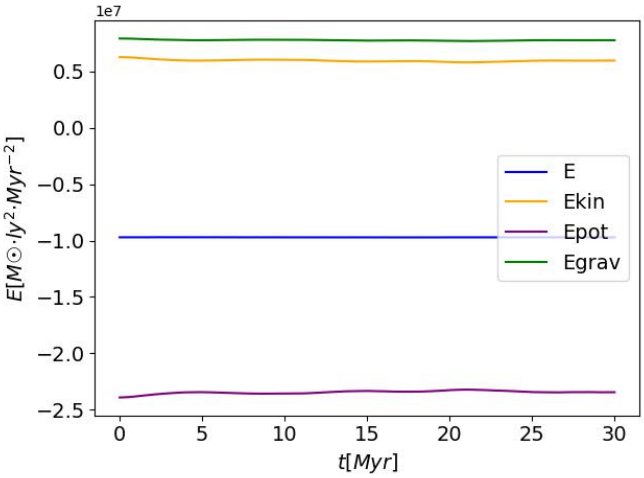

Figure 13: *Evolution of the energy through time. Egrav is the gravitational energy, Epot the potential energy, Ekin the kinetic energy and E the total energy. Simulation in deep MOND of NGC 5466*

Fig 13 shows that indeed the total energy remains very constant throughout the calculation, any fluctuation within potential and kinetic energy are compensated by fluctuations in the other. This supports that the simulations behave in a physical manner.

4.6 External Field Effect

The external field effect will most likely mainly be caused by the Milky Way, as all examined globular clusters are orbiting it. The Newtonian gravitational acceleration can easily be calculated and used as an indicator for the magnitude of the effect.

For NGC 6101 $a_{\mathrm{MW,N}} = 6.00 \cdot 10^{-11}$ m/s^2 $= 0.50$ a_0, and for NGC 5466, $a_{\mathrm{MW,N}} = 2.37 \cdot 10^{-11}$ m/s^2 $=$ 0.20 a_0.

Both these accelerations are below the threshold, so the acceleration in deep MOND would be a better indicator. For NGC 6101: $a_{\mathrm{MW,M}} = 8.49 \cdot 10^{-11}$ m/s^2 $= 0.71$ a_0. And for NGC 5466, $a_{\mathrm{MW,M}} = 5.33 \cdot 10^{-11}$ m/s^2 $= 0.44$ a_0.

The maximal acceleration in NGC 6101 is equal to A, so 1.04 a_0, and that of NGC 5466 is 0.569 a_0, so that the external field acceleration is 68 % or 77 % of the maximum Mondian acceleration caused by the body itself. It must be noted that, although the magnitude of the external field is quite large, it might still have little impact: according to the theory of relativity, the cluster should feel no gravity from the Milky Way when in orbit around it. This is how astronauts in ISS feel no gravity. This is contradictory to MOND, where the non-linear differential equations that relate the potential to the acceleration cause an external field to have a real impact on the distribution of the cluster. This means that it should at least be examined further and cannot be simply rejected.

Unfortunately, it was unfeasible to work out how this effect would impact the accelerations and execute the simulations using it within the scope of this thesis. However, other research, that could be expanded to the case of the isothermal sphere, has gone into this (Koster, 2024).

5 Results

Mass density distributions and velocity dispersions have been made and will be compared to the observed distributions of the clusters NGC 6101, NGC 6397 using different interpolations here.

5.1 Star count densities

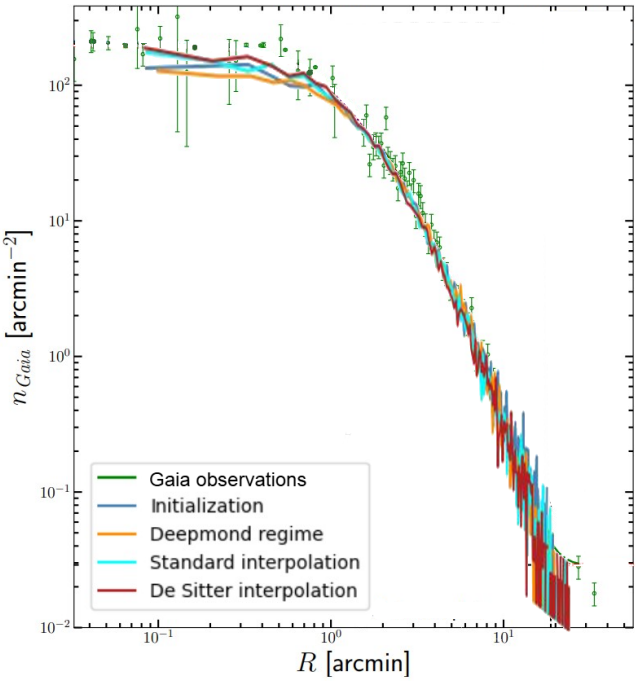

Figure 14: *2D projected simulated densities of NGC 6101 in number of stars per square arcminute against radius in arcminutes over observational data by (de Boer et al., 2019).*

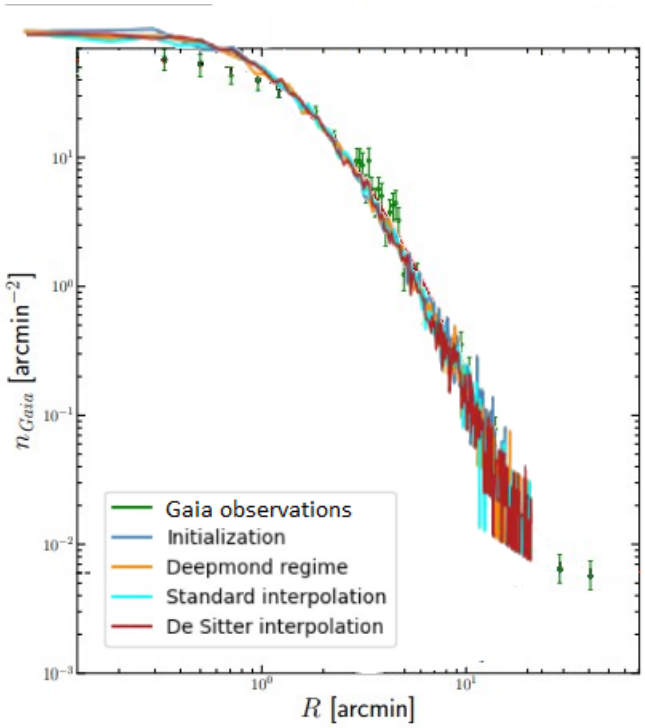

Figure 15: *2D projected simulated densities of NGC 5466 in number of stars per square arcminute against radius in arcminutes over observational data by (de Boer et al., 2019).*

The above density plot, Fig 14 shows the number of stars per square arcminute against the distance from the centre of the cluster in arcminutes. This is not the actual number of stars, but the number in the member selection of (de Boer et al., 2019). The star density has been determined using the ratio between the number of particles and the star count.

In the tail, the differences between the three regimes get overruled by the noise and it becomes impossible to tell which is best. In the centre, it can be seen that both interpolations are slightly closer to the data than deep MOND and the initialization are. The latter two simulations are slightly lower than the first few data points, and both interpolations are nicely on level. This is of course unsurprising, as the interpolations behave very similarly in both the centre and the tail, and only differ in the middle. Unfortunately, the differences between the two interpolations are quite small, so it is hard to tell which is better, but is seems as if the de Sitter interpolation is slightly closer.

Fig 15 shows that for NGC 5466 the MOND model does not fit as well. It must also be noted this set of observations was created from 42 % fewer stars than that of NGC 6101. The fit performed by (de Boer et al., 2019) showed the first point inside the flat density in the centre, but looking only at observations, it might not be impossible the simulations converge to the same point as the data.

Nonetheless, it seems here the simulation that produces the lowest density in the centre must be judged as the best, as the differences in the tail are again overruled by noise. The closest to the observations is now the standard interpolation, but only by a tiny difference. The de Sitter interpolation comes in second. The deep MOND simulation again comes in the last place.

It is also interesting to note that deep MOND performs a lot closer to the other two simulations for the cluster NGC 5466 than for NGC 6101, which is as expected, since NGC 5466 is more Mondian than the other. It reinforces the credibility of the results.

5.2 Velocity dispersions

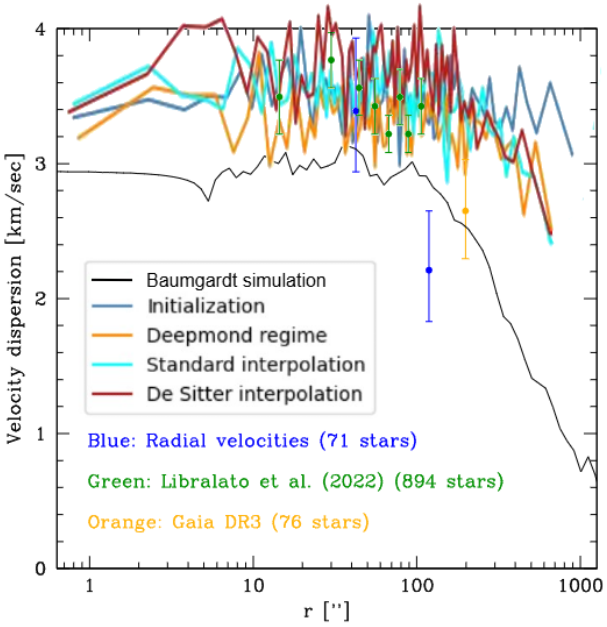

Figure 16: *1D velocity dispersions in km/s against radius in arcseconds of NGC 6101 plotted over the observed velocities by (Baumgardt et al., retrieved 2025)*

In Fig 16, it can be seen that the all simulations of the velocity dispersion for the cluster NGC 6101 match quite well to the observations in the region where the velocity dispersion is flat, and also considerably better than the Newton-based simulation by (Baumgardt et al., retrieved 2025).

The slope in the tail also seems to match, though this is based only on two observational points. Where the tail begins is significantly different: in all the simulations it begins at about 400 " and that of the observations begins at about 150". A potential explanation could be the same-mass particles: in a real cluster, the masses are distributed over an interval: 0.24-0.79 $M\odot$ in NGC 6101 and 0.21-0.78 $M\odot$ in NGC 5466 (Baumgardt et al., 2023). The rotation causes the most massive particles to move to the inside due to the equipartition of energy in an isothermal sphere. This changes the shape of the potential. No such effect occurs in the simulation.

With how close all three are compared to the noise in both simulated and observed data, this figure does not provide information regarding which function is the best.

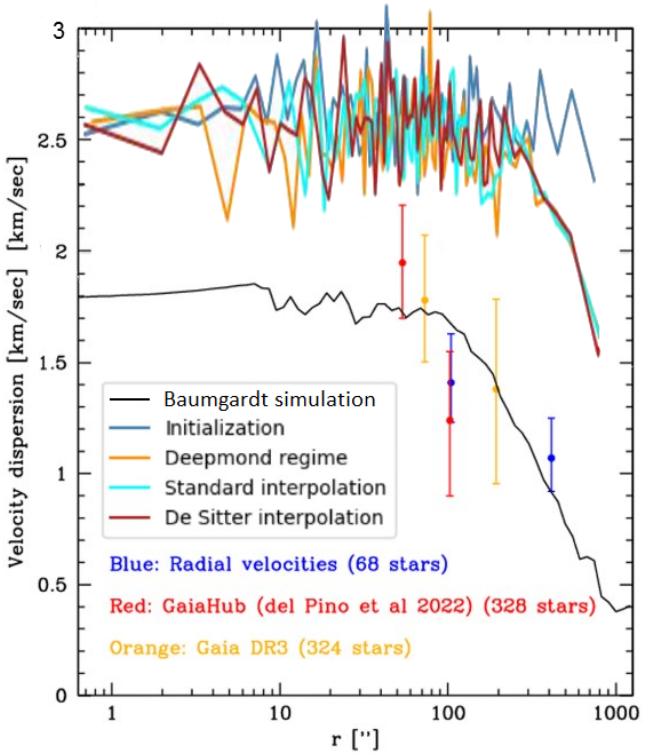

Figure 17: *1D velocities in km/s against radius in arcseconds of NGC 5466 plotted over the observed velocities by (Baumgardt et al., retrieved 2025)*

The simulated velocity dispersions of NGC 5466 do not match nearly as well as those of NGC 6101, and are all significantly higher (by a factor $\sim$ 1.3) than any observations (see Fig 17), where those of NGC 6101 matched very well in the central region. It can also be observed the tail starts much later in the simulations than in the observations again. (roughly 300" against roughly 100")

6 Discussion

Several of the obtained results are as expected, however, some are not. Here, potential causes of the discrepancies between the point where the velocity dispersion starts to decrease, in the value of the velocity dispersion in the flat region for NGC 5466, and in the central density of NGC 5466 will be discussed.

6.1 Generic causes

First a few generic causes for all issues will be discussed.

Generic causes like an incorrect total mass, or an incorrect half-mass radius are always possible, but hard to test or solve. By examining many clusters the chance all the data is wrong is reduced, and if the issues found here are found to be outliers, it follows

that indeed the input was wrong. However, this error could also be systemic, since all parameters have been found using Newton-based models. If the discrepancy caused by this is too large, the influence could be visible.

Another possible cause is of course that the MOND model is wrong. But since there are many other potential causes, this does not have to be the conclusion, especially since there is a lot that MOND does explain, both in this thesis and many other papers.

6.2 Velocity dispersion cutoff point

A potential cause for the discrepancy in radius where the velocity dispersion starts to decrease in both systems is the use of much higher masses than can be expected to be found on average in the clusters: in NGC 5466, for example, the stars vary between 0.21 and 0.78 $M\odot$ (Baumgardt et al., 2023), whereas they are simulated as all having a mass of 5.9 $M\odot$. In an inertial system, the most massive particles will move to the outside. The presence of more massive particles in the simulation could cause them to move further out than they do in the real cluster, causing the velocity dispersion drop-off at a later point. This is, however, contradicted by the well fitting distribution of stars.

A small discrepancy could be caused by smoothing out the particles: the standard deviation of each particle's mass spread is 1 pixel. This means the whole system gets extended by about 1 pixel in each direction. This might slightly move the cutoff point away from the centre, by 1 pixel. That corresponds to roughly 15 arcseconds for both systems.

6.3 Central velocity dispersion of NGC 5466

Here, there are several potential causes for the factor ~ 1.3 between observed and simulated velocity dispersions. It must be noted that the observed velocity dispersions might not yet be constant in the first few points. It is hard to tell with so few data. If the velocity is already decreasing in the innermost point, that would imply there is an even larger discrepancy in cutoff point.

A second potential cause is the initial velocity, derived from the isothermal sphere solution. A certain amount of energy is given to the system and this total energy will not change because there is no interaction with any external system. There is no guarantee this amount of energy is correct. If this initial energy is indeed too high, it is only a logical conclusion that the kinetic energy could linger in a too high state as well. Future research could attempt to construct an initial state based on observations of mass and velocity distribution.

It would also be possible the difference between the two clusters is caused by the external field effect of the Milky Way, if NGC 5466 would be closer and thus experience a stronger effect. This is not the case, however. It is possible that there is another cluster near NGC 5466 that causes a stronger external field effect than NGC 6101 is subject to, causing the discrepancy in the velocity dispersion for this cluster and not the other.

6.4 Central star density of NGC 5466

The density of stars in the centre of NGC 5466 matches somewhat to the data, but is ever so slightly higher. A bit further away, between 200-300', the simulated density is a bit lower than observed. From this, it can be estimated the total mass checks out and the usage of a different value for it can't be the cause.

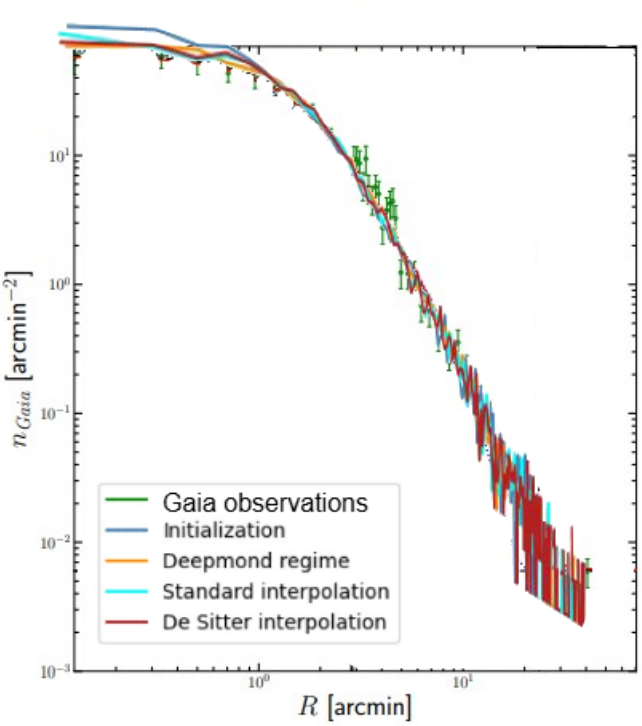

Figure 18: *2D projected simulated densities of NGC 5466, simulated with $b = 0.05 \cdot \frac{L}{2}$ in number of stars per square arcminute against radius in arcminutes over observational data by (de Boer et al., 2019).*

A potential cause is the ratio between the quarter-mass radius and the size of the box, which

influences resolution as well as the smoothness of the distribution. Fig 18 shows that for $b_{\text{frac}} = \frac{1}{20}$, the distribution matches better to the observational data than for $b_{\text{frac}} = \frac{1}{10}$, like in Fig 15. The higher resolution should improve the results but if the distribution isn't yet smooth enough, the behaviour of the system might be non-physical. It has been assumed so far that Fig 12 showed the distribution was smooth enough, but this is unproven. To improve smoothness, future research could attempt the same simulation with a larger number of particles.

Then there is the use of same masses for all particles. In a real cluster, the stars have a distribution of masses, and it is possible the stars are moved closer to or further from the centre based on their mass. In the approximation of the isothermal sphere for deep MOND, kinetic energy should be equal for all stars because of the thermodynamic equilibrium, meaning the most massive ones move at lower speeds and are thus in lower orbits. This means there would be less stars per unit of mass in the centre, which could explain the discrepancy in the graph.

Another potential cause is the mismatch between observed and simulated quarter-mass radii, as demonstrated by table 2. Since the simulated clusters are always smaller than the real ones, this could cause an increase in density in the centre. However, this effect should be larger for NGC 6101 than for NGC 5466, because in that cluster, the difference is larger.

served data points match very well to the simulation for NGC 6101, except for the last two. Because of the large noise within both observational and simulated data, no distinction can be made in quality of the two interpolations. In NGC 5466, all simulations produce too high velocity dispersions, and none of them edges closer to the data, so no conclusion can be drawn which works best.

It must also be taken into account that all used simulation input parameters have been processed using Newton-based models, influencing the simulations. Mistakes in the observations or calculation of parameters are also possible, in which case the poor matches found could be outliers.

Other potential causes, related to errors in the simulation, include limited resolution, limited number of particles, equal masses at a wrong value, and the energy given to the system by the initial state.

All in all, this research has been insufficient to conclude whether the de Sitter interpolation or the standard interpolation is superior. It can be concluded, however, that the de Sitter interpolation is on par with the standard function for isothermal spheres and should be considered as a viable alternative because of its ability to match both observations and the models using the standard function, as well as because of its relation to the shape of the universe and the physical meaning that it holds.

7 Conclusion

7.1 Conclusion from these results

The goal of this research has been to compare the de Sitter interpolation function to the standard interpolation function for globular clusters, approximated as isothermal spheres.

Fig 14 shows the two are, as expected, better than the deep-MOND case, but there is very little difference between the two interpolations. It does look like the de Sitter function matches slightly better.

Fig 15 gives somewhat less affirming results, even though it shows that all three simulations are now very close together, which is expected since this cluster is better approximated by deep MOND. The issue is that all three are further from the observations than the simulations of NGC 6101 were. This time, it looks like the standard function is slightly better.

The velocity dispersion again is simulated better for cluster NGC 6101 than for NGC 5466. All ob-

7.2 Future research

Future research could look into more clusters to see if either of the two examined has been an outlier, and also examine the regime of stars with a larger Newtonian component to ensure the interpolation works well for all kinds of clusters.

With a more powerful computer, or a larger amount of time, it could also be examined what a higher resolution (through more pixels or a larger b_{frac}) could achieve, combined with a larger number of particles to maintain smoothness and a larger number of timesteps to maintain stability.

The validity of the initial state should be further examined because the amount of energy given to it influences the final state as well. It could be attempted to calculate first the root mean square velocity and use it as an initial state.

The influence of the external field effect should also be examined.

8 Appendices

8.1 Appendix A: explosion of particles

The explosion of particles, meaning the average velocity suddenly increases dramatically and all particles leave the system, can be seen below. The total simulated time of the simulation in Figs 19 and 20 is 500 Myr, meaning all particles simply left the system early on.

Not all instances of particles exploding have looked like this, some would stabilize after suddenly increasing. Some would explode much faster, sometimes already at the first timestep. It has not succeeded to recreate these failed attempts.

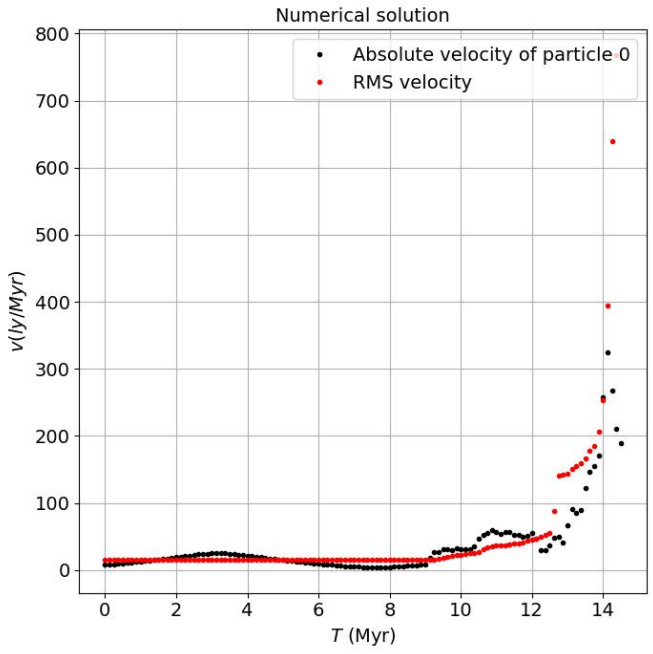

Figure 19: *v_{RMS} of the system and absolute velocity of an arbitrary particle in it. Cluster is NGC 5466 in the de Sitter interpolation with poorly chosen timestep size and b_{frac}.*

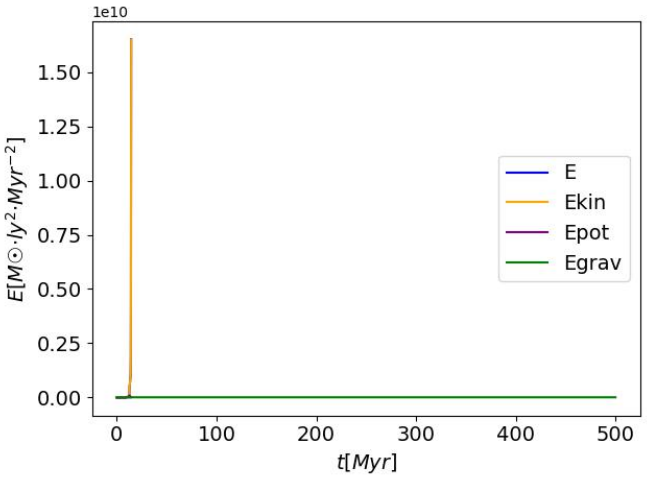

Figure 20: *Energies of the system. Cluster is NGC 5466 in the de Sitter interpolation with poorly chosen timestep size and b_{frac}.*

Parameter	Value
Simulated time	500 Myr
Timesteps	4000
Iteration steps	4
Number of particles	10 000
b_{frac}	0.2
Halfpixels	32

Table 4: *Example of poorly chosen parameters*

8.2 Appendix B: PC specs

The PC used for all the simulations in this thesis is one with the following components:

CPU: Intel(R) Core(TM) i5-10400F CPU @ 2.90 GHz

GPU: NVIDIA GeForce RTX 2060 (6 GB)

RAM: 16.0 GB (2x 8.0 GB)

Used storage drive: SSD 256 GB PCS PCIe M.2

Operating system: Windows 10 64-bits

8.3 Parameters used in simulation

Parameter	Value
Simulated time	30 Myr
Timesteps	6000
Iteration steps	4
Number of particles	10 000
b_{frac}	0.1
Halfpixels	64

Table 5: *Simulation parameters used in all simulations.*

Cluster	Total mass [10^4 M⊙]	Half-mass radius [pc]	Galactocentric distance [kpc]	Distance to Sun [kpc]	Number of stars [-]
NGC 6101	17	13.87	10.360	14.450	1750
NGC 5466	5.6	13.75	16.480	16.120	1007

Table 6: *Cluster parameters used in the simulations.*

References

Astroweb. Cold dark matter and experimental searches for wimps, retrieved 2025. `https://astroweb.case.edu/ssm/darkmatter/WIMPexperiments.html`.

H. Baumgardt, V. Henault-Brunet, N. Dickson, and A. Sollima. Evidence for a bottom-light initial mass function in massive star clusters. *Montly Notice of the Royal Astronomical Society, 000, 1–16 (201x)*, 2023.

H. Baumgardt, A. Sollima, M. Hilker, A. Bellini, E. Vasiliev, V. Henault-Brunet, and N. Dickson. Baumgardt database, retrieved 2025. `https://people.smp.uq.edu.au/HolgerBaumgardt/globular/`.

T. J. L. de Boer, M. Gieles, E. Balbinot, V. Henault-Brunet, A. Sollima, L. L. Watkins, and I. Claydon. Globular cluster number density profiles using gaia dr2. *Monthly Notices of the Royal Astronomical Society, Volume 485, Issue 4, June 2019, Pages 4906–4935*, 2019.

J. V. de Nijs, P. M. Visser, and S. W. H. Eijt. Fast particle-mesh code for milgromian dynamics. *Astronomy and Astrophysics, vol. 681, A90*, 2024.

J. Koster. Bsc thesis: Analyzing wide binary orbit stability with mond theory and external field effects. *TU Delft Repository*, 2024.

F. Lelli, S. S. McGaugh, J. M. Schombert, and M. S. Pawlowski. One law to rule them all: The radial acceleration relation of galaxies. *The Astrophysical Journal, 836, 152*, 2017.

T. Licquia and J. Newman. Improved constraints on the total stellar mass, color, and luminosity of the milky way. *American Astronomical Society, AAS Meeting 221, id.254.11*, 2013.

J. Madson. Finite-mass isothermal spheres and the structure of globular clusters. *Monthly Notices of the Royal Astronomical Society, Volume 280, Issue 4, pp. 1089-1093.*, 1996.

S. S. McGaugh. Stacy mcgaugh - missing mass and modified dynamics, 2021a. `https://youtu.be/DrGa7kMZzq0?si=4_7dlHdtwFJ8BtL8`.

S. S. McGaugh. Testing galaxy formation and dark matter with low surface brightness galaxies. *Studies in History and Philosophy of Science, Vol. 88, P. 220-236*, 2021b.

S. S. McGaugh, F. Lelli, and J. M. Schombert. The radial acceleration relation in rotationally supported galaxies. *Phys. Rev. Lett., Vol. 117, issue 20, P. 201101*, 2016.

M. Milgrom. A modification of the newtonian dynamics: implications for galaxies. *Astrophysical Journal, Vol. 270, p. 371-383*, 1983b.

M. Milgrom. The modified dynamics as a vacuum effect. *Physics Letters A, Vol. 253, Issues 5-6, p. 273-279*, 1999.

M. Milgrom. Mond- a pedagogigal review. *Acta Phys.Polon. B32 (2001) 3613*, 2001.

M. Milgrom. The mond limit from space-time scale invariance. *The Astrophysical Journal 698:1630-1638,2009*, 2009.

M. Milgrom. Ultra-diffuse cluster galaxies as key to the mond cluster conundrum. *Monthly Notices of the Royal Astronomical Society 454, 3810–3815 (2015)*, 2015.

M. Roshan, I. Banik, N. Ghafourian, I. Thies, B. Famaey, E. Asencio, and P. Kroupa. Barred spiral galaxies in modified gravity theories. *Monthly Notices of the Royal Astronomical Society, Vol. 503, Issue 2, p. 2833–2860*, 2021.

L. Smolin. Four principles for quantum gravity. *arXiv:1610.01968*, 2016.